ACCEPTED MANUSCRIPT

Multi-Meron Interactions and Statistics in Two-Dimensional Materials

To cite this article before publication: Xiaobo Lu et al 2022 J. Phys.: Condens. Matter in press https://doi.org/10.1088/1361-648X/ac671c

Manuscript version: Accepted Manuscript

Accepted Manuscript is "the version of the article accepted for publication including all changes made as a result of the peer review process, and which may also include the addition to the article by IOP Publishing of a header, an article ID, a cover sheet and/or an 'Accepted Manuscript' watermark, but excluding any other editing, typesetting or other changes made by IOP Publishing and/or its licensors"

This Accepted Manuscript is © 2022 IOP Publishing Ltd.

During the embargo period (the 12 month period from the publication of the Version of Record of this article), the Accepted Manuscript is fully protected by copyright and cannot be reused or reposted elsewhere.

As the Version of Record of this article is going to be / has been published on a subscription basis, this Accepted Manuscript is available for reuse under a CC BY-NC-ND 3.0 licence after the 12 month embargo period.

After the embargo period, everyone is permitted to use copy and redistribute this article for non-commercial purposes only, provided that they adhere to all the terms of the licence https://creativecommons.org/licences/by-nc-nd/3.0

Although reasonable endeavours have been taken to obtain all necessary permissions from third parties to include their copyrighted content within this article, their full citation and copyright line may not be present in this Accepted Manuscript version. Before using any content from this article, please refer to the Version of Record on IOPscience once published for full citation and copyright details, as permissions will likely be required. All third party content is fully copyright protected, unless specifically stated otherwise in the figure caption in the Version of Record.

View the article online for updates and enhancements.

Multi-Meron Interactions and Statistics in Two-Dimensional Materials

Xiaobo Lu¹, Linghan Zhu¹, and Li Yang^{1, 2*}

¹Department of Physics, Washington University in St. Louis, St. Louis, MO 63 30, USA.

²Institute of Materials Science and Engineering, Washington University in St. Louis, MO 63130, USA.

Abstract

As a fundamental type of topological spin textures in two cinensional (2D) magnets, a magnetic meron carries half-integer topological charge and for the a part with its antithesis to keep the stability in materials. However, it is challenging to transference of the characteristic highly inhomogeneous spin textures. In this work, we develop a discrete method to address the concentrated spin structures around the core of merors. We reveal a logarithmic-scale interaction between merons when their distance is larger than twice their core size and obtain subsequent statistics of meron gas. The model also predicts how these properties of single and paired merons evolve with magnetic exchange interactions, and the results are in excellent agreement with the Monte Carlo simulations using the parameters of real 2D van der Waals magnetic materials. This discrete approach not only shows equilibrium static statistics of meron systems but also is useful to further explore the dynamic are erties of merons through the quantified pairing interactions.

Migrating the concept of soliton from particle physics to condensed matter physics, the to regical solitons, such as skyrmions and merons, have attracted tremendous interests in magna tracing back to several decades ago because of their potential applications for mantu. inform ition and storage. ¹⁻⁶ With substantial experimental advances in recent years, such types of none linear spin textures have been observed in various material platforms, e.g., magne material surfaces, disks, and thin films within a wide range of temperature. ^{7–16} The formal or erons merely requires an in-plane O(2) magnetic anisotropy and does not demand any specific type of interactions, such as frustrated symmetric exchange interactions or the antisymmetric Dzyaloshinskii-Moriya (DM) interaction which stabilize the skyrmions. ^{17,18} Therefore, merons could be one of the common topological solitons in low-dimensional at weak spin-orbit coupling (SOC) magnetic systems. 19–21 More recently, the newly emerging as a fically thin two-dimensional (2D) magnets may work as the neat and natural playground for such topological spin textures. ^{22–} ²⁵ There are numerous experimental measurements byting heron states through suppression or large fluctuations of magnetic orders especially for monolayer structures. For example, the suppressed antiferromagnetic (AFM) order of no. layer NiPS3 was reported, and the XY features were discussed in monolayer CrCl₃. ^{26,27}

A systematic theoretical exploration is highly demanded in light of the recent experimental achievements in exploring topological spin textures. The strict 2D planar magnetic vortices and antivortices are known as the BK physics and have been heavily studied for decades^{28,29}. For the topological merons in the natural material, the in-plane geometry of the magnetic vortices and antivortices are inherited. However, unlike the strict 2D model, the out-of-plane spin texture is presented around the core gion to lower the free energy of meron in realistic materials. Current studies about merca son ans mainly focus on the structure and stability of bimerons in the frustrated ferromagne's (M) or chiral AFM monolayers as well as their dynamical responses under external spin currents or magnetic fields within the Landau-Lifshitz-Gilbert framework. ^{21,30}– ³⁴ The acc te description of the structural properties of single meron is limited, which is, however, the foundation for studying bimerons and further collective interactions. To date, most previous works followed the continuum analysis that has been successful in describing skyrmions. For e structure of a single meron was mimicked through the micromagnetic simulations exan. OOMMF package) accompanied by the continuum analysis³⁵, and its stability was also

discussed through a continuum model based on the Heisenberg Hamiltonian with the DM interaction included³⁶. However, different from skyrmions, merons typically exhibits the more compact core structures and form complicated networks in real materials. As pointed out in the seminal work of G. M. Wysin¹ about 2D easy-plane ferromagnets, the region close to the cortex geometry center cannot be described well by a continuum field. This is because the rapid variation of magnetic moments at the core represents a singularity in the continuous perspective. These characters make the continuum approach contentious to describe general properties of merons. Finally, the statistical distribution of the distance between merons is another determining property of the integrative multi-meron networks in materials, whereas there has been barely rigorous investigation about this fundamental trait in realistic materials. If this regard, it is worth endeavoring to find a general model to describe the thorough profile. Individual merons and their pairs.

In this paper, we develop a discrete model to study the equilibrium meron properties based on a Heisenberg Hamiltonian that takes the onsit at votropy and nearest neighbor (NN) exchange interactions into account. By constructing the soliton profile of both single and paired merons based on discrete lattices, we obtain the optimal core size, pair interaction, meron distance distribution and their evolution with the characteristic exchange interaction strength. The Above model results agree well with the on-interfering Monte-Carlo (MC) simulations. Thus, this discrete soliton method gives rise to a general way to study merons in practical materials and provide a comprehensive picture of low temperature meron statistical properties

Hamiltonian and similation setup. We consider the following XXZ-type Heisenberg Hamiltonian with the NN xchange interaction (J) and effective onsite anisotropy (A) to describe 2D magnets:

where \vec{m} represents the magnetic moment. Our previous study shows that the NN approximation produces agreement with the experiment and can predict the characteristic transition temberature of monolayer chromium trihalides within an error bar of several Kelvin. Hexagonal lattices are utilized in this study because most currently synthesized 2D magnets belong to this space. To mimic realistic materials, we initially set these parameters close to the effective

values of monolayer $CrCl_3$: the values of the effective onsite anisotropy A and Hormberg exchange constant J are 35 μeV and -790 μeV , respectively, which are obtained by fire principal calculations²⁰. We have to address that the effective anisotropy A takes into account both the magneto-crystalline anisotropy and the shape anisotropy (magnetic dipolar interactions), and its positive sign results in the in-plane O(2) symmetry which is crucial for realizing merons while prohibiting the formation of long-range magnetic orders at finite temperates. This peroximation can capture the essential meron physics while dramatically simplify the model and corresponding MC simulations. Utilizing monolayer $CrCl_3$ as the starting point we will keep A fixed while scanning J within a reasonable range to predict the meron proporties in general 2D magnets. In other words, we mainly focus on the exchange interaction and the rank of J/A, to avoid scanning a vast parameter space while grasping the essential physics ³⁹

Based on the Hamiltonian in Eq (1), we perform MC implant as via the Metropolis algorithm on 2D hexagonal lattices with a size of 240x240 hexagonal unit cells (if not particularly specified), which contains 115,200 magnetic moments. The periodic boundary condition is implemented in the MC simulations. A MC step consists of an attempt to assign a new random direction in three-dimensional (3D) space to one of the random magnetic moments in the lattice, and the acceptance ratio is setting via the vanilla Metropolis method. All magnetic moments are set to point along the out-of-plane direction at the initial across to mimic the experimental cooling condition with the help of an external field. Such initial setting warrants the overall zero topological numbers of system. The temperature of MC is fetting to $\kappa_B T = J_0/36$ to get a unclouded meron profile from thermal blurring. We run 2.304 ×10.0 MC steps in total (averaged 2 × 10⁵ steps per magnetic atom) to ensure the equilibrium state is reached.

Single meron. We sext from the merons in monolayer $CrCl_3$, a 2D magnet expected to be promising to loke in-plane reagnetic polarizations and merons. Figures 1 (a) and (b) present the schematic top-and side views of merons obtained from MC simulations of monolayer $CrCl_3$ using the DFT-c liculated J and A as mentioned above. These figures reveal a few fundamental characters of merons. First, the spin texture has a wave-pocket-like core with the $\pm \hat{z}$ direction spin component while the easy-plane spin components form the vortex or anti-vortex swirling around $\frac{11}{2}$ (11) Secondly, under ideal conditions, the in-plane swirling of a meron/anti-meron

extends to infinity until it is terminated by the system boundary or anti-meron/mero. These features are different from many other widely studied topological spin textures, such a transmission or magnetic bubbles which are self-contained.^{5,42} For example, a general studied sky train can be decomposed into an inner core, an outer domain, and a domain wall separating the sore an outer domains as plotted in the inset of Figure 1 (b).^{6,38,43}

To quantitatively describe a single meron, we have calculated its to ological charge that has been widely employed to characterize the topological properties of spin textures.⁵ The topological charge is defined as $Q = \int q(\vec{r}) = \int \frac{1}{4\pi} \vec{n} \cdot \left(\frac{\partial \vec{n}}{\partial x} \times \frac{\partial \vec{n}}{\partial y}\right)$, 44,45 the unit vector of local magnetic moment \vec{m} . The schematic topological charge distriction $q(\vec{r})$ of a meron in monolayer CrCl₃ is shown in Figure 1 (c). In this study, the integrate topological charge of the considered merons and anti-merons belongs to the half integer class (1). The half integer topological charge supports the idea that merons have to form park a stablize in an integer topology number form, which agrees with previous studies and observations. 2,16 Moreover, the most topological charge is condensed around the small core regio. As snown in Figure 1 (c), the diameter of the 5% isoline of the maximum value of local topological charge is about 4 nm, which is the length of 6 lattice constants because the in-plane lattice constant of $CrCl_3$ is about $6.01 \mbox{Å}^{20}$. This is much smaller than the skyrmions observed in $Fe_{0.5}C_{0.5}Si$, n, which the core size is around 90 nm. 9 In addition to the topological charge, we have so carculated the magnetic energy distribution based on the 1). In Figure 1 (d), the magnetic energy profile shows the similar Heisenberg Hamiltonian (E features as the topological charge distribution: most magnetic energy is condensed around the core region within a diagree. 7 nm. These results conclude that a manifest character of merons is their highly inhomomeneous spin texture around the core. The condensed core dominates most their energetic and topological properties of the single meron texture. This feature distinguishes mion, in which the topological charge is allocated around domain wall far merons from the away from the soliton center. Interestingly, such highly inhomogeneous spin textures of meron are To carry binary information based on the out-of-plane spin direction of cores and can be man valate by external field pulse, which is not achievable for the strict 2D planar vortexes. ¹⁵ On

the other hand, as we will show in the following, such highly inhomogeneous spin textures also bring difficulties in describing and quantifying merons through the traditional continuous alysis

The first step is to build a modeled profile function to describe the spin texture or single, eron.

Inspired by the hyperbolic secant form of the optic solitons⁴⁶, we construct the profile function to

describe the meron geometry:

$$\Phi(\phi) = \nu \phi + \delta \qquad (2)$$

10
$$\Theta(\mathbf{r}) = \frac{\pi}{2} - \arctan\left[\frac{1}{\sinh\left(\frac{r}{w + a_0}\right)}\right]$$

where $\Phi(\phi)$ and $\Theta(r)$ are the azimuthal

direction of a magnetic moment \overline{m} on the polar poorts ate $r(r, \phi)$ (illustrated in Figure 1 (a)), i.e., $\overline{m} = m_0 \left(sin(\Theta) cos(\Phi), sin(\Theta) sin(\Phi), cos(\Phi) \right)$. In Eq. (2), δ is the phase factor varying from 0 to 2π describing the swirling. We refer positive vorticity v to a meron and negative v to an antimeron. In this work, we restrict the discussion to |v| = 1, which is the most common and fundamental meron state with $\pm \frac{1}{2}$ topological charge, although |v| > 1 can still exist if considering specific excharge interactions beyond NN. ⁴⁷ In Eq. (3), a_0 is the lattice constant of magnetic lattices. w is large at the end of the meron core region, and it is the only tunable parameter

les, respectively, which describe the

Next, we employ the deron soliton profile in Eqs. (2) and (3) to tune the parameter w for obtaining the ground state (lowest) energy based on the Hamiltonian in Eq. (1). One popular way to evaluate such energy is the use the continuum approximation: 2,36,43,48

in this model. We can conso w with the widely used full width at half maximum (FWHM)

marked in Figure 1.b). For the soliton form in Eq. (3), FWHM = $2 ln(2 + \sqrt{3}) w \approx 2.63 w$.

$$E = \int \int \left(A' m_z^2 + \frac{J'}{2} |\nabla \overrightarrow{m}|^2 \right) dS \tag{4}.$$

A' and J' are treated as the continuous effective coefficients related with Eq. (1), and a notablized coefficient is necessary to ensure the proper unit of those micromagnetic anisotropy a constants since the second exchange term has a real-space gradient square. That g lient souare needs a factor of the area of a unit cell, which is $\sqrt{3}/2$ in hexagonal lattices (the artice co can be chosen as one since the ratio is relevant). Moreover, there are two magnitic Cr atoms (spins) in one unit cell, which gives another factor of 2. As a result, we need a semalize coefficient of $1/\sqrt{3}$ to A'/I'. This approach has provided gratifying results for describing kyrmions.⁴³ (See section 1 of the Supplemental Information for the detailed analysis of F (4) and corresponding boundary effect) In Figure 2 (a), we present the radial profile of a rons is monolayer CrCl₃ from the continuum model (the dash line) and the MC simulation, the dots. Unfortunately, compared with the MC result, the core size calculated by the continual moderns apparently underestimated. This deviation is from the fact that the main structures of perons, such as the topological charge distribution and the out-of-plane spin texture, are mady concentrated and dramatically varied around the center of the soliton within a fe am clos to the singularity point of the continuum treatment. This can be seen from Figure 1 (b) in which sharp variations of the spin texture are observed within a small-sized core.

To overcome such deviation in faced by the singularity at the meron core, we can deal with the discrete degrees of freedom of the veron in hexagonal lattices applying the profile function, without the continuum approximations. Following this idea, we discretize the single meron profile function (Eqs (2) and (3)) based on magnetic Bravais lattices and obtain the corresponding energy by directly following the factorized Hamiltonian in Eq (1). Via the procedure of energy optimization, the discretized peroach provides a very good portrait for the meron comparing with the observed merculinstance in the low-temperature ($k_B T = J_0/36$) MC simulation of monolayer CrCl₃ evidenced by the presement between the red solid line and dots in Figure 2 (a). Meanwhile, such a good agreement also corroborates the validation of our proposed soliton formula in Eq. (3) for descriping merons.

Then we go beyond monolayer $CrCl_3$ to check this discrete approach for general materials. We have the lated the single-meron profile by changing the exchange interaction J within a following like the latest profile and the single-meron profile by changing the exchange interaction J within a following like the latest profile and the single-meron profile by changing the exchange interaction J within a following like the single-meron profile by changing the exchange interaction J within a following like the single-meron profile by changing the exchange interaction J within a following like the single-meron profile by changing the exchange interaction J within a following like the single-meron profile by changing the exchange interaction J within a following like the single-meron profile by changing the exchange interaction J within a following like the single-meron profile by changing the exchange interaction J within a following like the single-meron profile by changing the exchange interaction J within a following like the single-meron profile by changing the exchange interaction J within a following like the single-meron profile by changing the exchange interaction J within a following like the single-meron profile by changing the exchange interaction J within a following like the single-meron profile by changing the exchange interaction J within a following like the single-meron profile by changing the exchange interaction J within a following like the single-meron profile by changing the exchange interaction J within a single-meron profile by changing the exchange interaction J within a single-meron profile by changing the exchange interaction by the single-meron profile by th

the exchange interaction strength of monolayer $CrCl_3$). The results are summarized in Fig. 2. (b). The model based on the discrete soliton solution (Eq. 3) always provides satisfactory g_1 amends with MC results within such a wide range of magnetic interactions. Moreover Figure 1. (b) reveals the trend of merons core associated with the exchange interaction. For example, g_1 are ger exchange interaction will increase the core size of merons. This is similar to the characteristic length scale increase as $\sqrt{J/A}$ in common magnetic domain wall structures. Such a treat is consistent with the understanding that a larger exchange interaction g_1 (in principle, g_2), increases the energy cost of forming in-plane swirling at the core region and makes the spins of the g_2 direction. Consequently, the soliton favors a broader span of the spin variations along g_2 and thus a larger core size. It is worth mentioning that this trend is opposite as everal size shrinkage against the increasing g_2 in skyrmions. When the exchange g_3 increases g_4 increases of the inner region of skyrmions overlays the thickness increase of the domain wall involving the DM interaction, resulting in an overall decreased size of skyrmions.

Figure 2 (c) summarizes the FWHM of meron, can lated by the three approaches, i.e., simulated from MC, optimized from the continuous and the discrete approaches based on profile function, for a wide range of exchange interaction J. As explained above, the continuum approach neglects the lattice discretization effect abound the core even truncated with a_0 avoiding the singularity and consequently underestimates the size of the meron soliton. In contrast, by introducing the lattice discretized profile function, the theoretical prediction of meron size is in good agreement with the MC simulation which is non-interfered method with the model.

Finally, it is worth mentions withat the meron core size is relatively robust against the distance between them. Figure 2 (d) lisplays the MC results of merons' the out-of-plane (\hat{z}) spin component under the different pair listances ranging from 10 to 40 nm observed in simulations of monolayer CrCl₃. The soliton profiles are nearly the same within the wide range of distance. Notable, the persistence of meron core structure against the pair distance emphasizes the importance of the discrete model of capturing the meticulous structure of the meron core region and verifies the feasibility of studying the interactions among merons through the rigid particle supposition, which will be as zed in the following bimeron profile and multi-meron statistics.

Bimeron profile. Unlike a skyrmion which maintains an integer topological charge itself usingle meron only carries half-integer topological charge and shows up in pairs, so-called topological states, to ensure the system belongs to the integer topological class. Hence, their pairs properties are worth being studied. Based on the in-plane geometry of vortex and anti-vortex swirm $x^{11,29}$, the spin moment $(m(\theta, \varphi))$ of a bimeron can be written as Eq. (5) based on the single meron profiles illustrated in Figure 3 (a):

7
$$\begin{cases} \theta = z^{+}\theta^{+}(r - r^{+}) + z^{-}\theta^{-}(r - r^{-}) \\ \phi = \gamma^{+}\phi^{+}(r - r^{+}) + \gamma^{-}\phi^{-}(r - r^{-}) + \delta \end{cases}$$
 (5)

where we label the meron and anti-meron via the superscripts by the in-plane swirling type: γ^+ 1 for vortex and $\gamma^-=-1$ for anti-vortex, the corresponding yearicities are contained in angles φ^\pm . r^+ and r^- are the core locations of meron and anti-meron (z^-) indicates the spin direction of the meron (anti-meron) core along the positive (+1) or newtive (+1) z-axis. The overall sign of the integrated topological charge of a single meron (anti-norm), decided by the product of its core vorticities γ which is $N = \frac{1}{2}\gamma z = \pm \frac{1}{2}.^{14,16}$ For the region spin direction z and in-plane swirlin bimerons discussed in this work, there are three class of the overall topological index (0 and ± 1). imulation conveniently, we mainly focus on the To corroborate results with experiment and class 0 configurations (as illustrated in Figure 1 (b)) where the spin z-direction of the cores in meron and anti-meron are the san. This configuration can be smoothly transferred from the fieldinduced FM state that could be easily wized in experiments and MC simulations because the conservation of the topological number and the initial setups of the perfect FM order in simulations. Since we only consider the socropic exchange and onsite anisotropy, the phase factor δ can be an arbitrary value between (2π) and gives the same degenerated energies. For example, in Figure 3(b) we present the structure appearance of meron pairs with four typical values of δ , i.e., $0,\frac{1}{2}\pi$, π , and $\frac{3}{2}\pi$, wich are observed in the MC simulations. ^{11,16}

With the above meron pair profile function, we can evaluate the pair interaction energy against the distance ($a = -r^- | r^- |$) between meron and anti-meron by using the discrete method established in the bimelon profile Eq.5. First, we begin with merons in monolayer CrCl₃. Figure 3 (c) presents the results obtained by the discrete (dots) approach. An attractive interaction is observed between r eros, and anti-meron. A logarithm curve (dashed line) excellently fits the results for $d > 2r_0$.

Interestingly, the Yang-Mills equations, which originally proposed meron-pair quasipal sles in
 high-energy physics, derives the similar logarithm-scale energy variation.^{3,4}

Such a logarithm scale can be understood by analyzing the asymptotic behavior to away it in the center ($|r| \gg |d|$) via the continuum analysis which is well established in the BKT physics. ^{28,29} Due to the highly concentrated meron profile, the corresponding asymptotic interaction between meron and anti-meron mainly comes from the region far from the cores. Thus, J is dominated by the exchange interaction of in-plane swirling of local magnetic moments since the highly localized core region does not contribute to the interaction between meror and anti-neron instances by the short-range Heisenberg exchange. To capture the primary scaling of invarction, the energy can be estimated as $E = \frac{J'}{2} \iint \nabla \vec{m} \cdot \nabla \vec{m} \, dS$. Combined with the panel prome (Eq. (5)), we could get the asymptotic energy expression as: (The details can be noted in Section 2. of the Supplemental Information)

$$E = J'\pi[(\gamma^+ + \gamma^-)^2 \ln \frac{b}{a_0} - 2\gamma^+ \ln \left(\frac{d}{a_0}\right)] \quad , (6)$$

where L is the system size. For bimeron states, $\gamma^+ + \gamma^- = 0$ and $\gamma^+ \gamma^- = -1$. Therefore, the first term is zero, and the residual second term continuous to a logarithm-scale energy between meron and anti-meron.

We must emphasize that, although the continuum treatment is helpful in understanding the asymptotic behavior, it cannot povide an accurate description for the strength of pair interaction. As discussed in the single beron hase, the center region of merons cannot be described by the continuum model, and an derivation of Eq. (6) is only asymptotically valid at the large r limit. Therefore, a discrepancy between the continuum model and discrete model should be expected. As shown in Figure 2 (c) the continuum analysis gives an overestimated interaction strength compared with the results can the discrete model, although both exhibit a logarithm scale.

When we study meron interactions, the potential is truncated at $2r_0$, where r_0 is the FWHM of the single-heron. Such a rigid core treatment for studying medium and long-range interactions at equilibrium state is supported by the MC simulations (Figure 2 (d)) which shows that the meron sore properties are barely affected by other merons that are apart larger than $2r_0$.

The attractive interaction between meron and antimeron is not directly associated with a chairing stability. The observed meron-antimeron pairs are essentially thermodynamic results at finite temperature. Beside the ferromagnetic ground state at zero temperature, at finite tax verature these quasi-orders with weak attractive interaction emerges from the Goldstone moths. ²⁸ In other words, we can imagine that some meron-antimeron pairs annihilate (disappear) vible other pairs emerge due to thermal fluctuations.

On the other hand, we must clarify that we constrain our study to the static profile of meron. Therefore, our approach is not able to describe the meron interaction when their cores overlap $(r < 2r_0)$, because the static profile model cannot grape the dynamic process such as the creation and annihilation of meron pair when they are nestling each other. In that situation, the meron profiles no longer follow the assumed soliton formula Eq. 3), while they are merging.

To expand our model and discussion to general makerials, we have calculated the meron/antimeron interactions with a range of exchange interaction (J), as shown in Figure 3 (d). For all the studied values of exchange interactions, the interaction energy retains the logarithm scale. Importantly, Figure 3 (d) shows that, as the exchange interaction J increases, the meron/anti-meron attractive interaction is enhanced. Because the total energy is proportional to the exchange interaction as seen from the An illtonian in Eq. (1).

Finally, the scaling law of peron pairing energy vs the system size is known to be important as it provides a scale guidanc for the experimental realization of meron solitons in the magnetic domains in natural insterials. 42,49,50 Unfortunately, the continuum solution confirms the energy convergence of the system 3 mentioned in Eq. (6) but it cannot provide the asymptotic behavior with varying system size. On the contrary, our discrete model reveals that the energy of a pair of merons with a fixed distance d converges as $1/L^2(\sim 1/N)$ to the system size, as shown in Figure 3 (e), and a system size of 240x240 unit cells are utilized in the study.

1 It is worth mentioning that the interaction between the same type merons or antimerons is a ulsive

However, without imperfections, such as magnetic defects, the conservation of the

number will forbid the instance of a single pair of the same type merons opanting ons. It real

materials, more than one pair of meron/antimerons can be thermally excited, which bring he to the

complex networks of merons/antimerons discussed in the following section.

Nearest neighbor (NN) distance of merons in materials. With the dispersion of interaction

8 energy shown in Figure 3 (d), more general meron behaviors, e.g. the response to the external

field and current induced torques^{5,30,31,34} can be studied through the subsequent macro soliton

effective models. In the following, we focus on the statistical properties of equilibrium meron pairs

in materials. Merons in materials can form complicated structures, such as the hierarchic structures

from "dipole like" to "quadrupole like" or even mo compleated networks. 12,20,30,51 These

topological defects networks were observed in MC qulations of monolayer CrCl₃, as shown in

Figures 4 (a) and (b). In such complicated network structures, we calculate the NN distance

between merons, ⁵¹ which is analogous to the visc see between meron and anti-meron in a simple

pair as discussed in the bimeron case. By examining the hyperbolic secant shape of the soliton

profiles, their vortex or anti-vortex in-plane swirling, and integrated half integer topological charge,

we can identify the meron type and its center ocation on the lattice with the help of a k-means

clustering algorithm, hence obtain NN distance.⁵² In this algorithm, we set the center of the

corresponding meron on the hexagonal latice site. This choice does not affect the result because

our simulation shows that the energy variation of different center position is negligible (~

 $10^{-4} \mu eV$) with a cell.

After collecting the ensemble of 1,360 distinct MC simulations, we generate the corresponding

25 statistical distribution (tb. NN distance shown as the histogram in Figures 5 (a)–(d) with different

exchange interaction J. In the rest part of this article, we will show that, using the bimeron

interaction brained above, we can develop a phenomenological model to capture the statistical

28 NN distance distribution in Figures 5 (a)-(d).

By in the NN model in 2D free gas, we start from a probability integration equation for

ti meron systems with the rigid core approximation.⁵³

$$f(r) = \left(1 - \int_{2r_0}^{r} f(r')dr'\right)\rho(r), \quad (7)$$

where f(r) represents the probability of finding an antithesis of a meron at the distance $\lambda \phi(r)$ represents the probability of the bimeron having a distance of r with one soliton fixed at the origin.

We further assume that $\rho(r)$ obeys the exponential relation with energy E(r), which can be obtained from the discrete meron pair profile in Figure 3 (d). Thus $\rho(r)$ can be written as $\frac{N}{Z} 2\pi r \, \mathrm{e}^{-\frac{E(r)}{E(2r_0)}}$, in which $E(2r_0)$ is the reference energy, and the normalization factor $Z_0 = \int_{2r_0}^{L} 2\pi r \, \mathrm{e}^{-\frac{E(r)}{E(2r_0)}} \, \mathrm{d}r$. N is the total number of merons achieved from MC simulations. By introducing the energy E(r) which can be obtained from the discrete meron pair profile in Figure

3 (d), we get the model describing the NN meron/anti-me on a sance from Eq (7)

12
$$f(r) = Z_1 r \frac{N}{z_0} \exp\left(-\frac{E(r)}{E(2r_0)}\right) \exp\left(-2\pi \frac{N}{r_0}\right) r' e^{-\frac{E(r')}{E(2r_0)}} dr', \quad (8)$$

where Z_1 is the normalization factor. A considering Figures 5 (a-d), this model is in good agreement with statistical results from MC simulation, especially under the long-distance condition. On the other hand, limited by the right-score assumption and neglecting possible merging process of merons and anti-merons, there are slight discrepancies at the small (short-range) distance. Nevertheless, the general agreement of our model with MC simulations in Figures 5 confirms that the discrete profile model not only vorks for single meron but also is suitable for studying multi-meron states in material, which expands the scope of the model.

Follow the same fort with single and bimeron studies, we have also studied the impact of the exchange interaction J to the NN distance of merons. An observed trend from Figures 5 (a) - (d) is that the large exchange strength J gives a shorter averaged NN distance and tighter distribution. Figure 5 (e) plots the highest probability distance and the averaged distance vs J. When J increases, the most package distance exhibits a decreasing trend. This is because a larger J results in stronger attractive interactions between meron and anti-meron as we discussed above. This will intrinsically lead to a smaller NN distance.

Finally, we must emphasize that, although the interaction energy between merons is labeled weak (Figure 3 (d)), this attractive interaction is significant in deciding the statistics of the ons. In figures 5 (a)-(d), we plot the result of the non-interacting free 2D gas in a dashed data. Without the weak attracting interaction, the most probable distance is substantially over stimated. For example, for monolayer CrCl₃ (Figure 5 (b)), the ideal gas model gives the most probable NN distance at 210Å while that from the discrete model is 116Å. Moreover, the width of the distribution of ideal-gas model is broader, resulting in a larger averaged NN distance of 267Å. The number is larger than the discrete model (169Å) because of the neglection of attractive interactions. The similar discrepancies are also observed at different exchange interaction J, as summarized in Figure 5 (e).

In summary, we built a discrete model in light of the serval discussion of planar 2D magnets¹ to explore the merons' general properties covering the ingle harons, meron pairs, and their lowtemperature equilibrium properties. By comparing vith the continuum approach and crossvalidating with MC simulation results, we ten estrate that such a discrete model accurately captures the important characters of meron solitons in 2D magnetic systems. The results confirm the discrete approach as a concrete way a explore topological meron properties and reproduce their interactions accurately that are crucial for understanding experimental measurements, such as the distance (correlation) distribution of dense nanoscale networks of merons and anti-merons surfaces.⁵¹ Furthermore, with the improved explicit interaction in 2D magnets and 3D magnetic from our discrete model, interesting models can be constructed to study the dynamic steries. This model would be useful for exploring the meron profile properties of merons in real of pinning, dragging, and paing in presence of moderate magnetic defects or external dynamic perturbations, which are a rectly connected with experimental realizations and further promising applications.

- **Supporting Information:**
- 2 Schematic illustration of meron energy and meron anti-meron asymptotical interaction and energy a
- 3 continuum approach (.docx)

- 5 AUTHOR INFORMATION
- Corresponding Author
- 7 *: E-mail: lyang@physics.wustl.edu (L. Y.)
- **8 Author Contributions**
- 9 L.Y. supervised the project. X.L performed the calculations and drafted the paper. All authors
- discussed the results and edited the paper.
- 12 Notes
- 13 The authors declare no competing financial interest.
- 15 ACKNOWLEDGMENT:
- 16 X.L. and L.Y. are supported by the Air Force Office of Scientific Research (AFOSR) grant No.
- FA9550-20-1-0255. F7 is seported by the National Science Foundation (NSF) grant No. DMR-
- 18 2124934. This wo suses the Extreme Science and Engineering Discovery Environment (XSEDE),
- which is supposed by ational Science Foundation (NSF) grant number ACI-1548562. The
- 20 authors acknowledge he Texas Advanced Computing Center (TACC) at The University of Texas
- 21 at Austin for providing HPC resources.



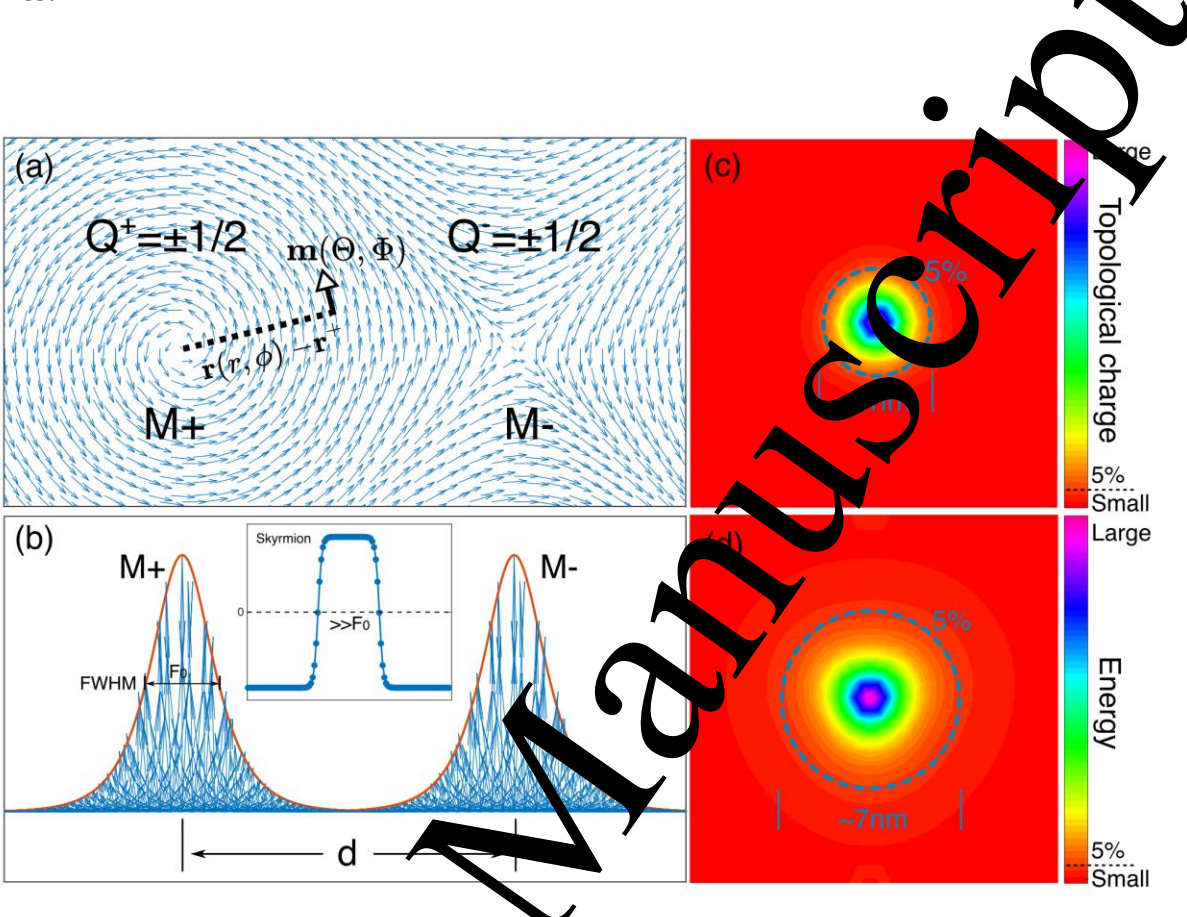
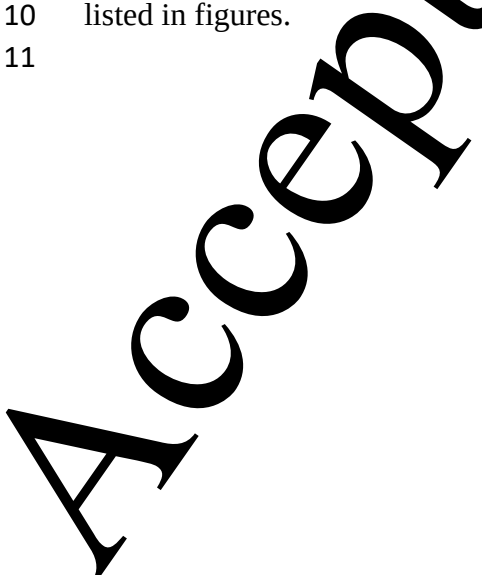


Figure 1 (a) Top view (in-plane charlity) of merons on 2D magnetic lattices. For the articulating purpose, meron and anti-meron are label by in-plane swirling types (M^+ for the vortex type and M^- for the anti-vortex type). The plan coordinate $\vec{r}(r,\phi)$ and m are illustrated in the dashed line and arrow, respectively (b) order view of merons. The inset is the structure of a skyrmion. (c) and (d) Schematic figures of the topological charge and energy distribution of a single meron. The dashed circle indicates a isolane with 5% of the maximal value and the estimated diameters are listed in figures.





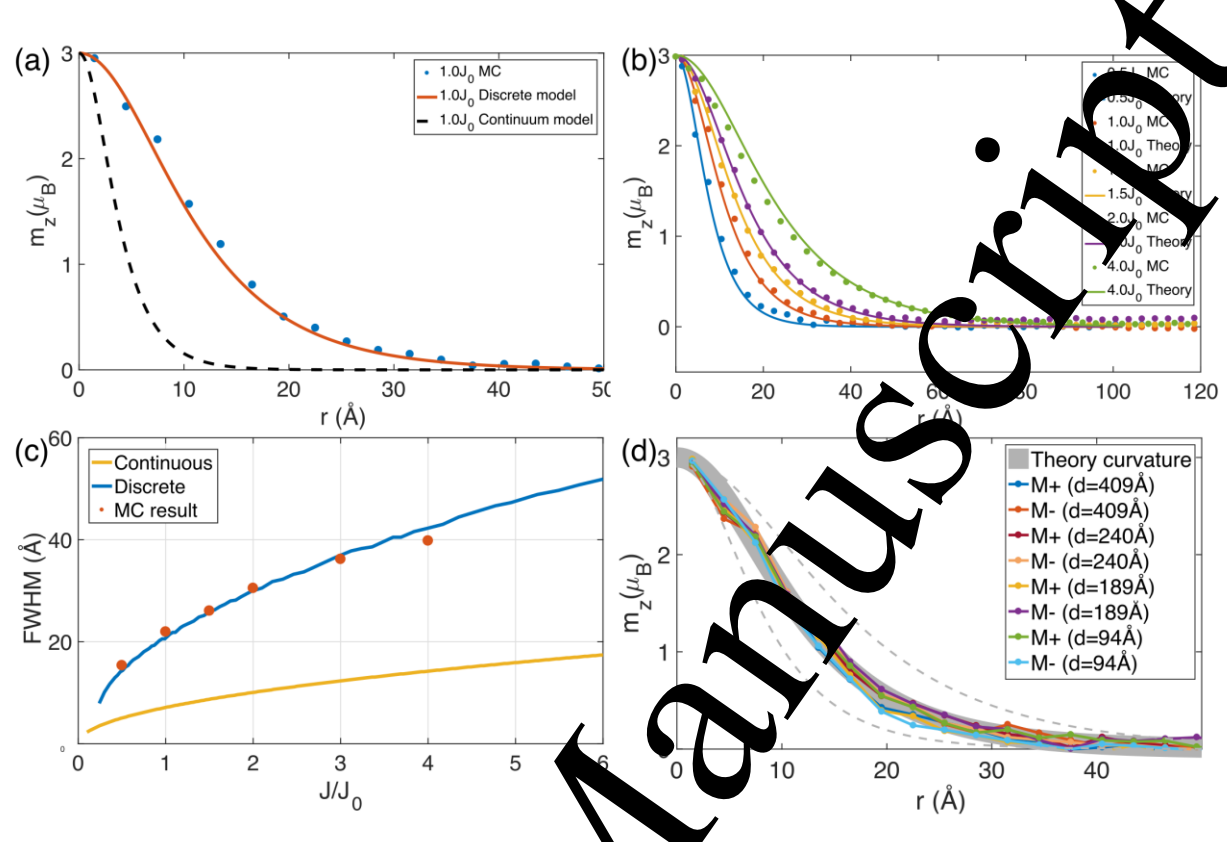


Figure2 Out of plane spin component (\hat{a}) of single meron profile. (a) Dots and lines are the MC simulated results and fitted profile theory results. (b) Comparison of the out of plane spin component (\hat{z}) from continuum model, discrete model and MC simulation under fixed $J = J_0$. (c) FWHM of single meron with ifferent J from continuum model, discrete model, and MC simulation. (d) Out-of-plane spin continuum (\hat{z}) of single meron extracted from MC simulation with the meron pair distance under a fixed $\hat{z} = J_0$. The dashed line indicates the curves of $\hat{z} = 0.5J_0$ and $\hat{z} = 2J_0$ from (b) to guidate adders—eyes.

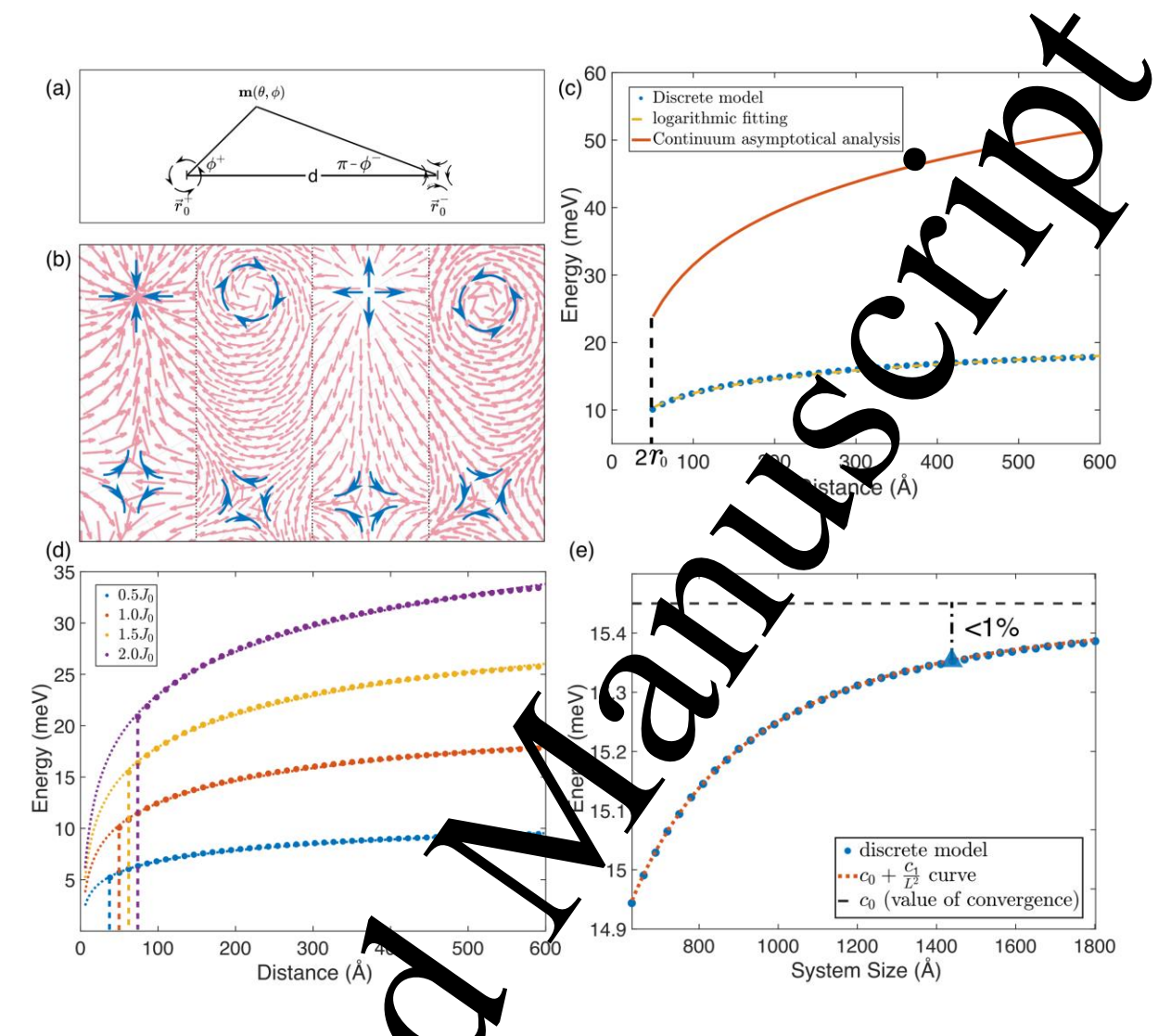
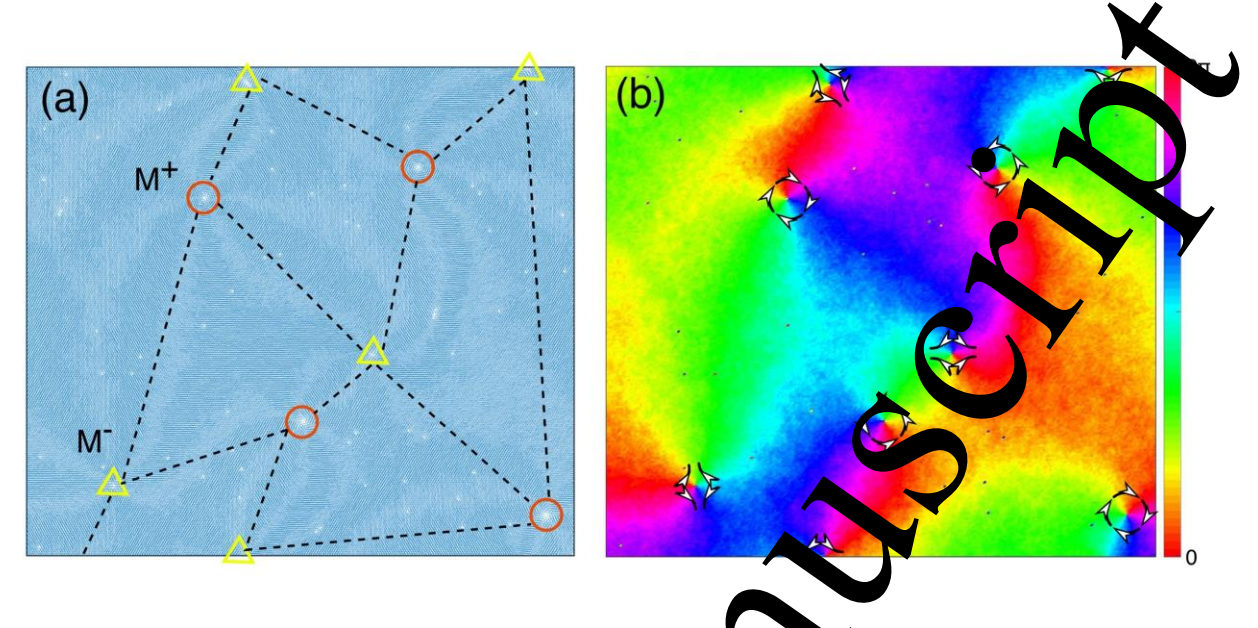
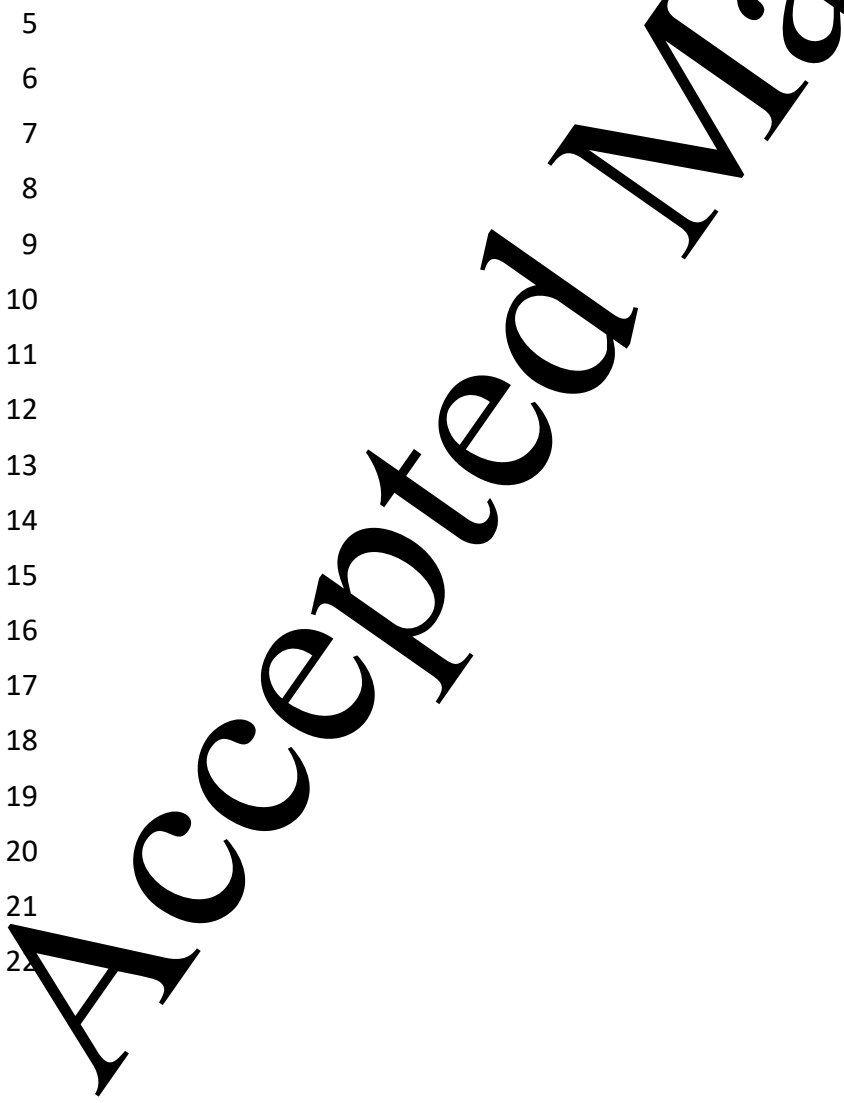


Figure3 (a) Schematic of a mero. and definitions of coordinates (b) Typical meron pairs observed in MC simulations with a phase factor δ close to $0, \frac{\pi}{2}, \pi, \frac{3\pi}{2}$. The in-plane swirling is marked in a 3x3 superval. (c) succon pair energy vs the distance between meron and anti-meron with a truncation at $2r_0$. (c) Simparison of pair energies with different exchange interaction J. The dot lines are the fitting logarithmic scale. (e) Convergence of meron pair energy against the system size at $J = r_0$ and fixed distance of 240Å.



sime ions of monolayer CrCl₃. The Figure4 (a) Schematic plot of meron networks from M merons and anti-merons are labeled by red circle (M⁺) and Now triangle (M⁻) (b) In-plane phase on are illustrated by arrowheads. map of (a). The swirling directions of meron and arti-r



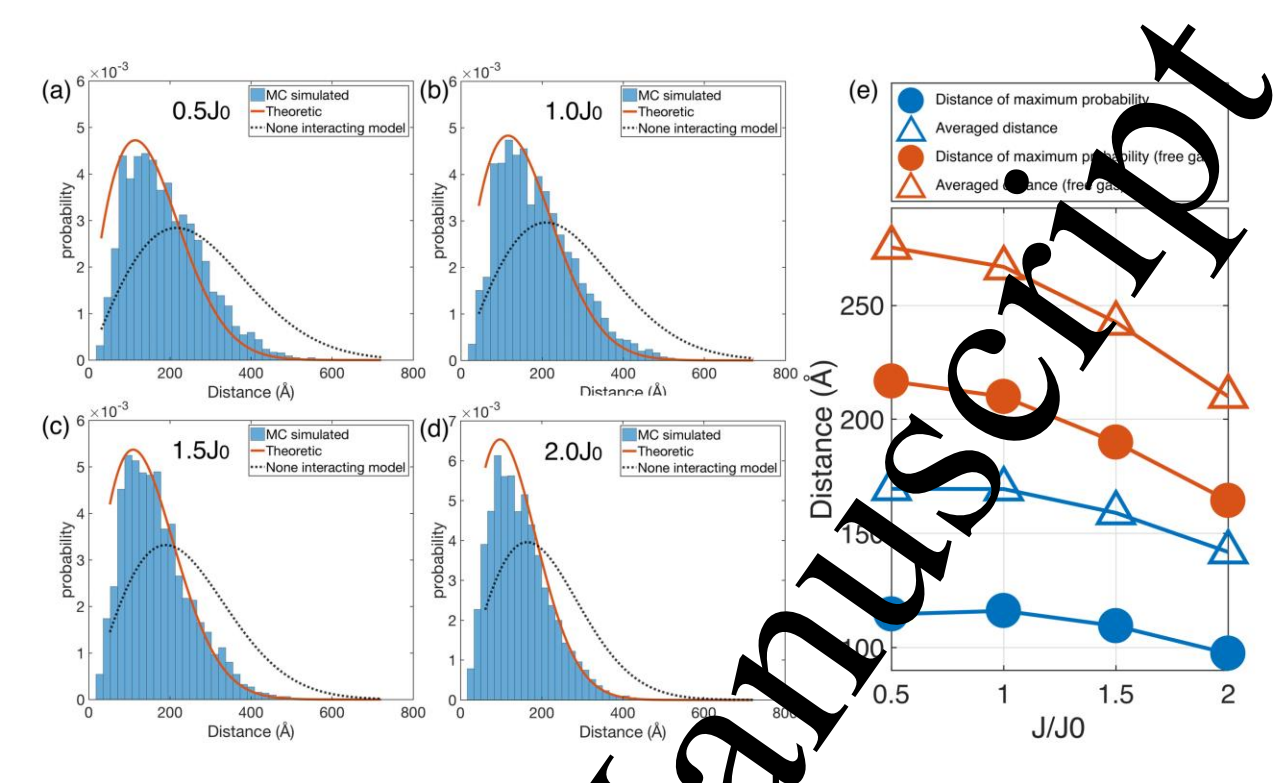
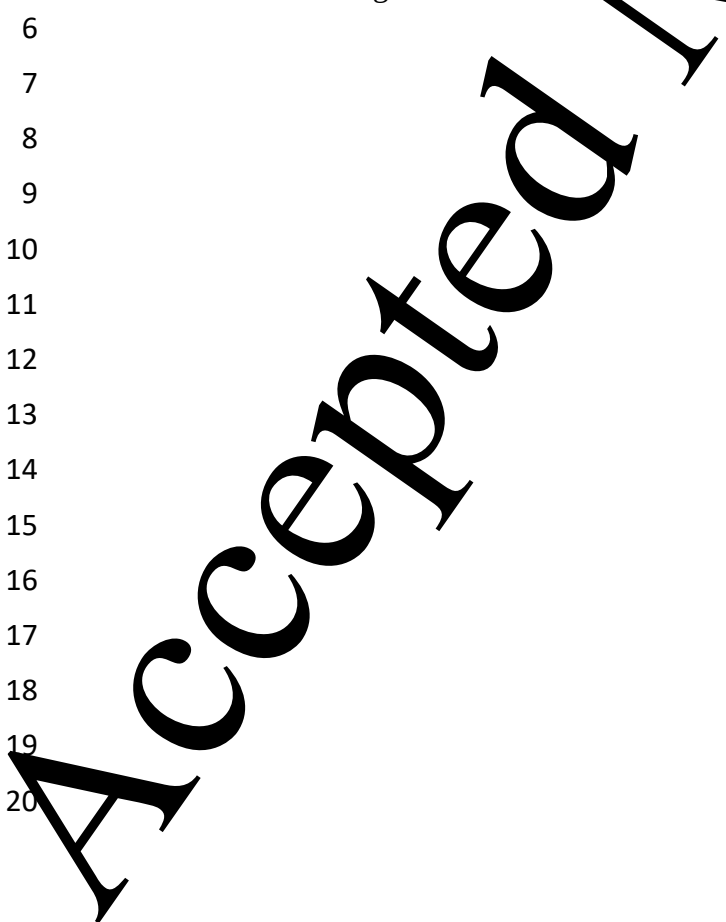


Figure5 (a-d) Distribution of the NN distant between plerons from MC simulations (the blue histogram), the discrete model (the red curve), uncone-interacting model (the black dashed curve) under different exchange interaction J. (e) Summary of the most probable distance and averaged distance vs the exchange interaction J.



REFERENCES:

- 2 (1) Wysin, G. M. Instability of In-Plane Vortices in Two-Dimensional Easy-Plane Ferromagnets. Phys. Rev. B **1994**, 49 (13), 8780–8789.

 4 https://doi.org/10.1103/PhysRevB.49.8780.
- 5 (2) Bogdanov, A. N.; Yablonskii, D. A. Thermodynamically Stable Vortice in A. gnetic. *Iy* 6 Ordered Crystals. Zh. Eksp. Teor. Fiz **1989**, 95, 178–182.
- 7 (3) Callan, C. G.; Dashen, R.; Gross, D. J. Toward a Theory of the Strong Inc. actions. Phys. Rev. D **1978**, 17 (10), 2717–2763. https://doi.org/10.1103/PhysRevD.17.2717.
- 9 (4) Actor, A. Classical Solutions of SU(2) Yang-Mills Theories. Rev. Mod. Phys. **1979**, 51 (3), 461–525. https://doi.org/10.1103/RevModPhys.51.461.
- Hellman, F.; Hoffmann, A.; Tserkovnyak, Y.; Beach, G. S. I ton, E. E.; Leighton, (5) C.; MacDonald, A. H.; Ralph, D. C.; Arena, D. A.; Dürr, H. A.; Fischer, P.; Grollier, J.; Yrivorotov, I. N.; May, S. J.; Heremans, J. P.; Jungwirth, T.; Kimel, A. V.; Koopmans, B., K.; Slavin, A. N.; Stiles, Petford-Long, A. K.; Rondinelli, J. M.; Samarth, N.; Schuler, M. D.; Tchernyshyov, O.; Thiaville, A.; Zink, B. L. Interfact induced Phenomena in Magnetism. Rev. Mod. Phys. **2017**, 89 (2), 02500**6**. https://doi.org/10.1103/RevModPhys.89.025006
- 18 (6) Rößler, U. K.; Bogdanov, A. N.; Pfleiderer, C. Spontar, ous Skyrmion Ground States in Magnetic Metals. Nature **2006**, 442 (7104), 197-8.

 20 https://doi.org/10.1038/nature05056.
- Mühlbauer, S.; Binz, B.; Jonietz, F.; Phele er, C.; Rosch, A.; Neubauer, A.; Georgii, R.;
 Böni, P. Skyrmion Lattice in a Chiral Magnet. Cience (80-.). 2009, 323 (13), 915.
 https://doi.org/10.1126/science 10.5048, 381-b.
- Neubauer, A.; Pfleiderer, C.; Binz, R.; Roscn, A.; Ritz, R.; Niklowitz, P. G.; Böni, P.
 Topological Hall Effect in the A Phase of MnSi. Phys. Rev. Lett. 2009, 102 (18), 186602.
 https://doi.org/10.1103/IL sRevLett.10Z.186602.
 - (9) Yu, X. Z.; Onose, Y.; Kanaza, a. N.; Park, J. H.; Han, J. H.; Matsui, Y.; Nagaosa, N.; Tokura, Y. Real-Space Observator of a Two-Dimensional Skyrmion Crystal. Nature **2010**, 465 (7300), 901–904. https://doi.org/10.1038/nature09124.
 - (10) Phatak, C.; Petford-Long, A. K.; Heinonen, O. Direct Observation of Unconventional Topological Spin Structure i Coupled Magnetic Discs. Phys. Rev. Lett. **2012**, 108 (6), 067205. https://www.org/s.com/o3/PhysRevLett.108.067205.
 - (11) Tan, A.; Li, J.; Sche A.; Arenholz, E.; Young, A. T.; Li, Q.; Hwang, C.; Qiu, Z. Q. Topology of A.; Meron Pairs in Coupled Ni/Fe/Co/Cu(001) Disks. Phys. Rev. B**2016**, 94 (1), 014433 https://coi.org/10.1103/PhysRevB.94.014433.
 - (12) Chmiel, F. P.; Vate field Price, N.; Johnson, R. D.; Lamirand, A. D.; Schad, J.; van der Laan, C.; Larris, D. T.; Irwin, J.; Rzchowski, M. S.; Eom, C.-B.; Radaelli, P. G. Observ von of Magnetic Vortex Pairs at Room Temperature in a Planar α-Fe2O3/Co Het Strucke. Nat. Mater. 2018, 17 (7), 581–585. https://doi.org/10.1038/s41563-018-0101-x.
 - (13) Yu, Y. 7 Koshibae, W.; Tokunaga, Y.; Shibata, K.; Taguchi, Y.; Nagaosa, N.; Tokura, Y. Transformation between Meron and Skyrmion Topological Spin Textures in a Chiral Mag et. Nature **2018**, 564 (7734), 95–98. https://doi.org/10.1038/s41586-018-0745-3.

- Pairs in Ferromagnetic Multilayer Elements. Phys. Rev. Lett. **2013**, 110 (17), 1772. https://doi.org/10.1103/PhysRevLett.110.177201.
- Van Waeyenberge, B.; Puzic, A.; Stoll, H.; Chou, K. W.; Tyliszczak, T.; Herte, R., Fähnle, M.; Brückl, H.; Rott, K.; Reiss, G.; Neudecker, I.; Weiss, D.; Back, L. H.; Schütz, G. Magnetic Vortex Core Reversal by Excitation with Short Bursts of an Alternation Field. Nature **2006**, 444 (7118), 461–464. https://doi.org/10.1038/nature/524
 - (16) Gao, N.; Je, S. G.; Im, M. Y.; Choi, J. W.; Yang, M.; Li, Q.; Wang, T.X.; Lee, X.; Han, H. S.; Lee, K. S.; Chao, W.; Hwang, C.; Li, J.; Qiu, Z. Q. Creation and Ann. Nation of Topological Meron Pairs in In-Plane Magnetized Films. Nat. Commun. **201**, 10 (1), 5603. https://doi.org/10.1038/s41467-019-13642-z.
- 11 (17) Okubo, T.; Chung, S.; Kawamura, H. Multiple-q States and the Skyn. on Lattice of the Triangular-Lattice Heisenberg Antiferromagnet under Magnetic Co. ls Tsuyoshi. Phys. Rev. Lett. **2012**, 108 (1), 017206. https://doi.org/10.1103/PhysRevLett.108.017206.
- 14 (18) Lin, S.-Z.; Hayami, S. Ginzburg-Landau Theory for Skyrmic s in Inversion-Symmetric
 15 Magnets with Competing Interactions. Phys. Rev. B 261, 93 (1), 064430.
 16 https://doi.org/10.1103/PhysRevB.93.064430.
 - (19) Xue, F.; Hou, Y.; Wang, Z.; Wu, R. Two-Dimensional L. sromagnetic van Der Waals CrC L3 Monolayer with Enhanced Anisotropy and Cur. Temperature. Phys. Rev. B **2019**, 100 (22), 1–7. https://doi.org/10.1103/PhysRevB.**1**23.2244.
 - (20) Lu, X.; Fei, R.; Zhu, L.; Yang, L. Meron-lik, Topolical Spin Defects in Monolayer CrCl3. Nat. Commun. **2020**, 11 (1). http://doi.org/10.1038/s41467-020-18573-8.
 - (21) Augustin, M.; Jenkins, S.; Evans, R. F. L., Tovoselov, K. S.; Santos, E. J. G. Properties and Dynamics of Meron Topological Sp., Textures in the Two-Dimensional Magnet CrCl3. Nat. Commun. **2021**, 12 (2019) https://doi.org/10.1038/s41467-020-20497-2.
 - (22) Huang, B.; Clark, G.; Navarro-Montalla, E., Klein, D. R.; Cheng, R.; Seyler, K. L.; Zhong, Di.; Schmidgall, E.; McGuire, M. A.; Cobden, D. H.; Yao, W.; Xiao, D.; Jarillo-Herrero, P.; Xu, X. Layer Dependent Ferromagnetism in a van Der Waals Crystal down to the Monolayer Limit. Nature. 917, 546 (7657), 270–273. https://doi.org/10.1038/nature225.
 - (23) Gong, C.; Li, L.; Li, Z.; Ji, S.; Storn, A.; Xia, Y.; Cao, T.; Bao, W.; Wang, C.; Wang, Y.; Qiu, Z. Q.; Cava, R. J., Louie, S. G.; Xia, J.; Zhang, X. Discovery of Intrinsic Ferromagnetism in Typ-Din ensional van Der Waals Crystals. Nature **2017**, 546 (7657), 265–269. https://doi.org/10.38/nature22060.
 - (24) Deng, Y.; Yu, Y.; S. 19, Y.; Zhang, J.; Wang, N. Z.; Sun, Z.; Yi, Y.; Wu, Y. Z.; Wu, S.; Zhu, J.; Wang J., Shen, X. H.; Zhang, Y. Gate-Tunable Room-Temperature Ferromagnetism in Two-Dimensional Fe3GeTe2. Nature **2018**, 563 (7729), 94–99. https://doi.org/1038/s41586-018-0626-9.
- Han, M.-G., Garlo, J. A.; Liu, Y.; Zhang, H.; Li, J.; DiMarzio, D.; Knight, M. W.;
 Petrovi, C.; Janiwala, D.; Zhu, Y. Topological Magnetic-Spin Textures in TwoDirections. Van Der Waals Cr 2 Ge 2 Te 6. Nano Lett. **2019**, 19 (11), 7859–7865.
 https://doi.org/10.1021/acs.nanolett.9b02849.
 - (26) Kih K.; Lim, S. Y.; Lee, J.-U.; Lee, S.; Kim, T. Y.; Park, K.; Jeon, G. S.; Park, C.-H.; Park J.-G.; Cheong, H. Suppression of Magnetic Ordering in XXZ-Type Anti-erromagnetic Monolayer NiPS3. Nat. Commun. **2019**, 10 (1), 345. https://doi.org/10.1038/s41467-018-08284-6.
 - Bedoya-Pinto, A.; Ji, J.-R.; Pandeya, A.; Gargiani, P.; Valvidares, M.; Sessi, P.; Radu, F.;

- Chang, K.; Parkin, S. Intrinsic 2D-XY Ferromagnetism in a van Der Waals Mono. er. Prepr. https://arxiv.org/abs/2006.07605 (2020). **2020**.

 Kosterlitz, J. M.; Thouless, D. J. Ordering, Metastability and Phase Transition in 1 o-
 - (28) Kosterlitz, J. M.; Thouless, D. J. Ordering, Metastability and Phase Transition in Po-Dimensional Systems. J. Phys. C Solid State Phys. **1973**, 6 (7), 1181–1203. https://doi.org/10.1088/0022-3719/6/7/010.
- (29) José, J. V. 40 Years of BKT Theory 2013.
 https://doi.org/10.1017/CBO9781107415324.004.
- Zhang, X.; Xia, J.; Shen, L.; Ezawa, M.; Tretiakov, O. A.; Zhao, G.; Liu, Y. Zhou, Y.
 Static and Dynamic Properties of Bimerons in a Frustrated Ferron agnetic Monolayer.
 Phys. Rev. B 2020, 101 (14), 144435. https://doi.org/10.1103/Phys RevB. 01.144435.
- 11 (31) Kim, S. K. Dynamics of Bimeron Skyrmions in Easy-Plane Magnets Lauced by a Spin Supercurrent. Phys. Rev. B **2019**, 99 (22), 224406.

 13 https://doi.org/10.1103/PhysRevB.99.224406.
- Li, X.; Shen, L.; Bai, Y.; Wang, J.; Zhang, X.; Xia, J.; Ezawa, M.; Tretiakov, O. A.; Xu,
 X.; Mruczkiewicz, M.; Krawczyk, M.; Xu, Y.; Evans, T. F. L.; Chantrell, R. W.; Zhou, Y.
 Bimeron Clusters in Chiral Antiferromagnets. npj Comput. F. ater. 2020, 6 (1), 169.
 https://doi.org/10.1038/s41524-020-00435-y.
 - (33) Zhang, X.; Xia, J.; Ezawa, M.; Tretiakov, O. A.; D. H. T.; Zhao, G.; Liu, X.; Zhou, Y. A Frustrated Bimeronium: Static Structure and Evnant, s. Appl. Phys. Lett. **2021**, 118 (5), 052411. https://doi.org/10.1063/5.0034396.
 - (34) Shen, L.; Li, X.; Xia, J.; Qiu, L.; Zhan, X.; Tre jakov, O. A.; Ezawa, M.; Zhou, Y. Dynamics of Ferromagnetic Bimerons Dh. p by Spin Currents and Magnetic Fields. **2020**, No. 1, 1–9.
 - (35) Radaelli, P. G.; Radaelli, J.; W. C. Ld. Proce, N.; Johnson, R. D. Micromagnetic Modeling and Imaging of Vortex | Leron Structures in an Oxide | metal Heterostructure. Phys. Rev. B **2020**, 101 (14), 144420. https://doi.org/10.1103/PhysRevB.101.144420.
 - (36) Bera, S.; Mandal, S. S. Theory of the Skyrmion, Meron, Antiskyrmion, and Antimeron in Chiral Magnets. Phys. Rev. **2019**, 1 (3), 033109. https://doi.org/10.1103/PhysRevi. earch.1.033109.
 - (37) Lu, X.; Fei, R.; Yang, L. C. ie Tomperature of Emerging Two-Dimensional Magnetic Structures. Phys. Rev B **.019**, 100 (20), 205409. https://doi.org/10.1103/Phys.levB.100.205409.
 - (38) Rohart, S.; Thia ide, A. C., rmion Confinement in Ultrathin Film Nanostructures in the Presence of Dzyalos, inskii-Moriya Interaction. Phys. Rev. B **2013**, 88 (18), 184422. https://doi.org/10.103/PhysRevB.88.184422.
 - (39) Ye, M.; Chalukov, L. V. Quantum Phase Transitions in the Heisenberg J1- J2 Triangular Antiferromagn, in A Magnetic Fiel. Phys. Rev. B **2017**, 95 (1), 014425. https://doi.org/10.103/PhysRevB.95.014425.
 - (40) Wacho vak, A; Wiebe, J.; Bode, M.; Pietzsch, O.; Morgenstern, M.; Wiesendanger, R. Dir Obstration of Internal Spin Structure of Magnetic Vortex Cores. Science (80-.). 2002, 298 (5593), 577–580. https://doi.org/10.1126/science.1075302.
 - (41) Shi a T Magnetic Vortex Core Observation in Circular Dots of Permalloy. Science (80-1). **2000**, 289 (5481), 930–932. https://doi.org/10.1126/science.289.5481.930.
 - (42) Malozemoff, A. P.; Slonczewski, J. C. Magnetic Domain Walls in Bubble Materials: A. Jances in Materials and Device Research; Academic press: New York, 1979.
 - Wang, X. S. R.; Yuan, H. Y.; Wang, X. S. R. A Theory on Skyrmion Size. Commun.

- Phys. **2018**, 1 (1), 31. https://doi.org/10.1038/s42005-018-0029-0.
- (44) Berg, B.; Lüscher, M. Definition and Statistical Distributions of a Topological Number the Lattice O(3) σ-Model. Nucl. Phys. B **1981**, 190 (2), 412–424. https://doi.org/10.1016/0550-3213(81)90568-X.
- (45) Wang, W.; Daniels, M. W.; Liao, Z.; Zhao, Y.; Wang, J.; Koster, G.; Rijnders, G., Guang, C.-Z.; Xiao, D.; Wu, W. Spin Chirality Fluctuation in Two-Dimensional Ferr, pagnet with Perpendicular Magnetic Anisotropy. Nat. Mater. **2019**, 18 (10), 1354–1059. https://doi.org/10.1038/s41563-019-0454-9.
- (46) Taylor, J. R. *Optical Solitons : Theory and Experiment*; Cambridge University Press, 1992.
 - (47) Zhang, X.; Xia, J.; Shen, L.; Ezawa, M.; Tretiakov, O. A.; Zhao, G., L., X.; Zhou, Y. Static and Dynamic Properties of Bimerons in a Frustrated Furniture and petic Monolayer. Phys. Rev. B **2020**, 101 (14), 144435. https://doi.org/10.1103/PhysR.vB.101.144435.
 - (48) Leonov, A. O.; Monchesky, T. L.; Romming, N.; Kubetzka, . Bogdanov, A. N.; Wiesendanger, R. The Properties of Isolated Chiral Sky, vious in Thin Magnetic Films. New J. Phys. **2016**, 18 (6), 065003. https://doi.org/10.1088/j.../7-2630/18/6/065003.
 - (49) Cullity, B. D.; Graham, C. D. Introduction to Magnetic Materials; John Wiley & Sons, 2011.
 - (50) Braun, H. B. Fluctuations and Instabilities of Fromas etic Domain-Wall Pairs in an External Magnetic Field. Phys. Rev. B**1994**, 50 (2.2) 16485–16500. https://doi.org/10.1103/PhysRevB.50. \$485.
 - (51) Eggebrecht, T.; Möller, M.; Gatzmann, V. Rubiano Da Silva, N.; Feist, A.; Martens, U.; Ulrichs, H.; Münzenberg, M.; Ropers, C.; Chäfer, S. Light-Induced Metastable Magnetic Texture Uncovered by Situ Larentz Microscopy. Phys. Rev. Lett. **2017**, 118 (9), 1–7. https://doi.org/10.1103/PrysRevLett.118.097203.
 - (52) Lloyd, S. Least Squares Quantization in PCM. IEEE Trans. Inf. Theory **1982**, 28 (2), 129–137. https://doi.org/10.1/20/TIT.1982.1056489.
 - (53) Bansal, P. P.; Ardell, A. J. Arage Nearest-Neighbor Distances between Uniformly Distributed Finite Particle. Meta. graphy **1972**, 5 (2), 97–111. https://doi.org/10.1016/002 0807 (72)90048-1.